Long-Range Electronic-to-Vibrational Energy Transfer from Nanocrystals to Their Surrounding Matrix Environment

Assaf Aharoni, Dan Oron, and Uri Banin*

Institute of Chemistry and the Center for Nanoscience and Nanotechnology, The Hebrew University of Jerusalem, Jerusalem 91904, Israel

Eran Rabani and Joshua Jortner

School of Chemistry, The Sackler Faculty of Science, Tel Aviv University, Tel Aviv 69978, Israel

(Received 3 October 2007; published 6 February 2008)

A radiationless transition process of long-range, resonance interconversion of electronic-to-vibrational energy transfer (EVET) is discovered between the band-gap excitation of nanocrystal quantum dots to matrix vibrational overtone modes using fluorescence lifetime measurements. A theoretical analysis based on long-range dipole-dipole nonadiabatic couplings, being distinct from the traditional adiabatic or ''static-coupling'' pictures, is given and is in qualitative agreement with experiments. EVET should be considered in matrix choices for near-infrared optoelectronic applications of nanocrystals.

DOI: 10.1103/PhysRevLett.100.057404 PACS numbers: 78.67.Hc, 78.67.Bf, 82.20.Ln

A ubiquitous and universal class of dynamic processes in large molecules, the condensed phase, and biomolecules encompasses radiationless electronic-to-vibrational energy conversion and vibrational energy exchange, which are central for the analysis, control, and optimization of energy storage and disposal in chemistry, physics, material science, and biology [1–4]. Electronic-to-vibrational energy transfer is an important example and pertains to intramolecular internal conversion and intersystem crossing and high spin–low spin conversion in molecules [1], nonradiative electron-hole recombination in semiconductors [2], small polaron motion [2], electron transfer and transport in solution [5] and in the photosynthetic reaction center and DNA [3,4], and resonance electronic energy transfer between large molecules [6,7].

In this Letter we report on the extension of the possible radiationless transition processes to include a novel case of long-range electronic-to-vibrational energy transfer (EVET). We provide experimental and theoretical evidence for dipole-dipole long-range, resonance, radiationless interconversion of core band-gap electronic excitation of semiconductor nanocrystal quantum dots (QDs) to C–H vibrational overtones of various matrices, which competes with the emission process. The proposed mechanism becomes possible due to the large transition dipole moment of the QD, which couples to the smaller transition dipole of the $(3n)$ overtone of the C–H vibrational stretch, sufficient to induce nonradiative transitions on time scales of the order of submicroseconds. Predictions of the size-dependent scaling law for the nonadiabatic rate based on Fermi's golden rule are provided along with comparisons between the theory and the experiments, revealing that the proposed long-range EVET mechanism is plausible. The EVET process is also of significance for the application of the QDs in near-infrared (NIR) optoelectronic devices [8–11] where proper matrix choice [12] is required to avoid undesired nonradiative processes.

To study QDs-matrix coupling we follow exciton recombination dynamics which are best reflected in the photoluminescence (PL) properties. Both PL intensity and lifetimes will be affected by the coupling, but monitoring the PL decay time is preferred over intensity based measurements, since it is not influenced by the direct absorption of the solvent and is less sensitive to experimental parameters. InAs/CdSe/ZnSe core-shell-shell (CSS) QDs [13] which display size-tunable NIR emission where C–H bending and stretching overtones of typical organic matrices are active, are investigated. The graded-shell structure creates an effective confinement potential minimizing nonradiative PL quenching via surface traps, and emission quantum yields (QY) of over 50% were achieved. This allows the PL measurements to be sensitive to coupling to matrix modes.

Typical environments for QDs are either solvents or polymer matrices. We compared two kinds of solvents: (a) 1,1,2-trichloro-1,2,2-trifluoroethane ($C_2F_3Cl_3$) and (b) toluene. The fluorinated solvent is used in comparison to the toluene to show the effect of C–H vibrations on the QDs PL properties. Two types of polymers are also compared: (c) perfluorocyclobutane [14,15] (PFCB) polymer and (d) poly(vinyl butyral-*co*-vinyl alcohol-*co*-vinyl acetate) (PVB).

Figure 1 shows emission and absorption spectra for 5.7 nm CSS-QDs in $C_2F_3Cl_3$ [Fig. 1(a)], where the QY is measured to be 60%, and in toluene where the QY is 50% [Fig. 1(b)]. The width of the PL spectrum is governed by the inhomogeneous size distribution of the QDs, where different core InAs sizes yield varying band gaps due to quantum confinement. The transmission spectrum of toluene [Fig. 1(c)] exhibits vibrational overtones around 1150 nm originating from aromatic and methyl C–H stretching modes that are assigned to the 1st $(2n)$ and 2nd $(3n)$ overtone transitions [16,17]. In toluene, the effect of the overtone absorption on the PL spectrum is seen.

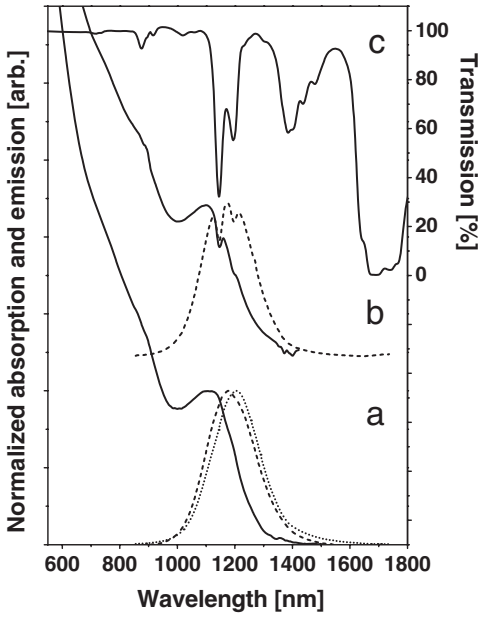

FIG. 1. Absorption (solid lines) and emission (dashed lines) spectra of 5.7 nm CSS-QDs in $C_2F_3Cl_3$ (a) and in toluene (b). The thin dotted line in (a) is the emission spectrum of the same particles in PFCB. The transmission spectrum of toluene is shown in (c). The C–H vibrational overtones at 1145 nm and 1195 nm are also observed as dips in the absorption and the PL spectra of the QDs in toluene.

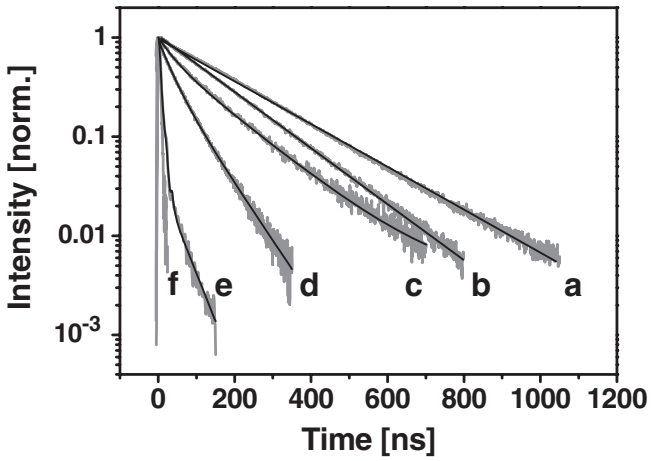

FIG. 2. Photoluminescence decay of the 5.7 nm CSS-QDs (a)–(d) in different matrices: ($C_2F_3Cl_3$) (a), PFCB polymer (b), toluene (c), and PVB polymer (d). PL decay of the 4.3 nm InAs cores in toluene is also shown (e), and (f) is the system response. The gray lines are the measured signals and the black solid lines are exponential fits. In (e) the black line is a convolution of the signal and the system response. (a) and (b) are single exponential. (d) is biexponential. (c) and (e) are triexponential. The extracted lifetimes (time for decay of PL intensity to $1/e$ of its initial intensity) are (a) 202 ns, (b) 154 ns (c) 98 ns (d) 45 ns, and (e) 3 ns.

Time resolved measurements of the emission decay at 1200 nm, overlapping the CH overtone band, are shown in Fig. 2. In the plain QD cores [Fig. 2(e)] the emission decay is very fast, close to the system response [Fig. 2(f)], due to rapid nonradiative decay via surface traps. In the CSS-QDs the decay is significantly longer in all the matrices demonstrating the effectiveness of the passivating shells in preventing PL quenching by surface traps. The decay in the CSS-QDs is still, however, significantly affected by the matrix, and the lifetimes range from 45 ns in PVB to 202 ns in $C_2F_3Cl_3$. In the $C_2F_3Cl_3$ solvent near-resonance matrix modes are absent, and the single exponential decay, with time constant τ_0, reflects best the behavior of the PL without matrix interactions. In contrast, toluene and PVB can interact with the CSS-QDs via an electronic-to-vibrational energy transfer between the exciton in the CSS-QDs and the C–H vibrational overtones of the matrix, explaining the shortening of the lifetimes.

To further probe this interaction we next compare lifetimes of CSS-QD particles in $C_2F_3Cl_3$ and toluene as a function of emission wavelength across the relevant CH overtone range (Fig. 3). A dominant observation is that in both solvents, τ increases with increasing detection wavelength. The steeper slope in the fluorinated solvent is due to the lower refractive index compared to toluene. As already noted, the main source for spectral broadening is the size distribution, and hence we can assign the lifetime at each wavelength to dominantly represent a specific core size.

We next consider the possible sources for the increasing lifetimes with larger particle size. Fermi's golden rule, from which a reciprocal relation between decay rates and emission frequencies can be deduced for QDs in the strong confinement regime, $\Gamma = \text{const} \times \omega$, where Γ is the rate constant ($\Gamma = 1/\tau$) and ω is the frequency of the emitted light [18], leads to an expected increase of only about 20% between 1000 and 1300 nm, much smaller than the observed increase from 40 ns for smaller particles (with 2.6 nm InAs cores) to 150 ns in the bigger particles (with 4.9 nm InAs cores). Examining the change in the electron-hole overlap integral of the smaller CSS-QDs emitting at 1000 nm compared to the bigger ones emitting at 1300 nm using effective mass approximation calculations showed negligible differences [19]. Another reason for the increase of τ with wavelength may be the switching of hole energy levels in the valence band, from an optically allowed one to a forbidden one, in the larger CSS-QDs [20–22].

Closer comparison of τ in toluene and the fluorinated solvent reveals clearly that the difference in lifetimes between the two is most significant near the position of the CH modes. In toluene a local dip is observed around 1150 nm followed by a flat region, and in the fluorinated solvent a flattening is seen at higher wavelengths. To better understand the effect of the CH overtone modes, in Fig. 3(b) we plot $\frac{k_T}{k_0} = \frac{\tau_0}{\tau_{\text{tol}}} \frac{n_0^2}{n_{\text{tol}}^2} - 1$, where k_T is the rate of the additional nonradiative channel in toluene, k_0 is the decay rate in the fluorinated solvent, and τ_0 and τ_{tol} are the

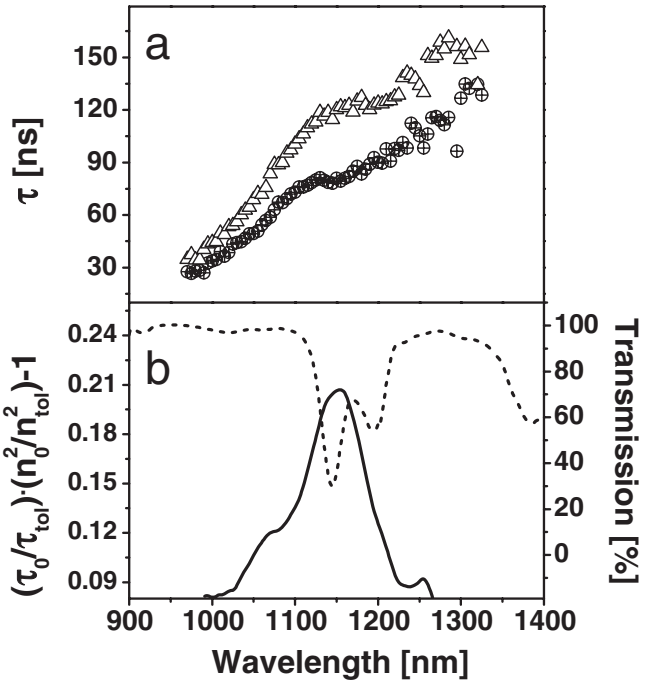

FIG. 3. (a) τ values of 5.2 nm CSS-QDs in toluene (filled circles) and in $C_2F_3Cl_3$ (open triangles) as a function of wavelength. (b) The relation between τ_{toluene} (measured in toluene) and τ_0 (measured in $C_2F_3Cl_3$) is indicated with a solid line. This is compared to the toluene absorption (dashed line).

measured lifetimes in the fluorinated solvent and toluene, respectively, corrected by the respective refractive indices, n_0 and n_{tol}. This representation eliminates the size effect on the lifetime. A resonance overlapping the C–H vibrational overtones is observed with maximal difference near 1145 nm matching the $3n$ overtone transition of the aromatic C–H stretching in toluene.

Before analyzing these results, we note that in both solvents the nanocrystals are overcoated with passivating organic ligands, which contain only methyl and methylene CH groups absorbing around 1195 nm. Plotting the ratio between the decay rates eliminates also the effect of the ligands.

Such resonant behavior is described by the following coupling and sequential decay scheme: $|\psi_I\rangle|\chi_{\{\omega\}}\rangle|\chi_{v=0}\rangle \overset{\hat{V}}{\leftrightarrow} |\psi_F\rangle|\chi_{\{\omega\}}\rangle|\chi_{v=3}\rangle \rightarrow |\psi_F\rangle|\chi_{\{\omega'\}}\rangle|\chi_{v=0}\rangle$, where the electronic wave functions $|\psi_I\rangle$ ($|\psi_F\rangle$) represent the initial core excited state (core ground state), $|\chi_{v=3}\rangle$ ($|\chi_{v=0}\rangle$) is the C–H bond-mode $v = 3$ vibrational state (ground vibrational state $v = 0$), $|\chi_{\{\omega\}}\rangle$ and $|\chi_{\{\omega'\}}\rangle$ are the nuclear states of all the other modes, and $\hat{V}$ is the coupling operator between the two states. The $|\psi_F\rangle|\chi_{\{\omega\}}\rangle|\chi_{v=3}\rangle$ state exhibits intrastate vibrational relaxation to a quasidegenerate $|\psi_F\rangle|\chi_{\{\omega'\}}\rangle|\chi_{v=0}\rangle$ vibronic quasicontinuum, which is induced by anharmonic coupling and mode mixing within the $|\psi_F\rangle$ vibronic manifold.

Several plausible energy transfer mechanisms should be considered, which are commonly treated using adiabatic (Born-Oppenheimer) or ''static-coupling'' (crude Born-Oppenheimer) methods [3,23–25]. In the former, one generates adiabatic potential surfaces, and transitions between these surfaces are due to the ''nonadiabatic'' coupling arising from kinetic energy terms of the surroundings. In the static-coupling method, the interaction between the dot or impurity and the surroundings involves shifted or distorted potential surfaces. The adiabatic and static-coupling methods are commonly used to describe *short-range* nonadiabatic transitions and can be excluded for inorganic nanostructures interacting with the surroundings due to the large separation between the core and the accepting mode of the matrix. This is particularly true for the present case where the accepting mode of the matrix is a localized CH vibration, and the electronic wave functions of the core QD are well isolated and at a distance of 2–3 nm from the surroundings by the passivating shells.

Instead, a long-range EVET is proposed induced by resonance electronic-vibrational dipole-dipole coupling. This picture extends the Förster model for electronic-electronic resonance energy transfer [6] to that of electronic-vibrational resonance energy transfer. We adopt a similar picture of the static-coupling method and write the Hamiltonian $\hat{H} = |\psi_I\rangle\hat{H}_I\langle\psi_I| + |\psi_F\rangle\hat{H}_F\langle\psi_F| + \hat{V}$, where H_I (H_F) is the initial (final) Hamiltonian of all nuclear degrees of freedom of the QD and the surroundings, and $\hat{V}$ is the coupling. In the static-coupling approach, the form of $\hat{V}$ involves shifted or distorted surfaces and high-order coupling schemes, which can be excluded for QDs as mentioned above. Instead, we adopt a picture where $\hat{V}$ is given by a multipole expansion of the Coulomb interactions between the electrons on the QD and the nuclear degrees of freedom of the surrounding. However, unlike the case discussed by Förster where the multipole expansion is in the electronic degrees of freedom of both the donor and the acceptor, here the expansion involves the electronic degrees of freedom of the donor (the QD) and the nuclear degrees of freedom of the acceptor (the C–H vibrational modes). In this scheme, the near-resonance coupling strength can be approximated to lowest order by $V = \frac{1}{\varepsilon R^3}\mu_{\text{el}}\mu_{\text{vib}}$, where $\mu_{\text{el}} = \langle\psi_I|\hat{\mu}_e|\mu_F\rangle$ is the core electronic dipole moment (for emission), $\mu_{\text{vib}} = \langle\chi_{v=0}|M_1Q + M_2Q^2 + M_3Q^3|\chi_{v=3}\rangle$ is the matrix C–H bond-mode vibrational transition dipole moment [26] [with the coefficients M_i ($i = 1$–3) being determined by the corresponding dipole moment derivatives], R is the distance between the nanoparticle and the accepting C–H mode, and $\varepsilon = n^2$ is the dielectric permittivity of the environment given in terms of the refractive index n. The EVET rate to a single C–H mode is given by Fermi's golden rule $\Gamma_{nr} = \frac{2\pi\kappa^2|V|^2}{\hbar\gamma}$, where γ^{-1} is the density of states; i.e., the homogeneous linewidth for the dissipation of the $v = 3$ C–H bond mode into lower frequency intra-

molecular and solvent modes [26], and $\kappa^2 = 2/3$ is a geometric factor [6]. The EVET from the excited core occurs in parallel to kN_s C–H bond modes on the nanoparticle surface, where $N_s = (R/d_0)^2$ is the number of molecules on the surface (with d_0 being their effective radius) and k is the number of accepting modes on a given molecule. The EVET rate $\Gamma_{\mathrm{EVET}} = kN_s\Gamma_{\mathrm{nr}}$ is then given by

$$\Gamma_{\mathrm{EVET}} = \frac{2\pi k\kappa^2}{\hbar d_0^2 n^4}\frac{|\mu_{\mathrm{el}}|^2|\mu_{\mathrm{vib}}|^2}{\gamma R^4}, \quad (1)$$

which scales like $\Gamma_{\mathrm{EVET}} \propto R^{-4}$ due to the cumulative effects of dipole-dipole coupling and the acceptor C–H bond packing on the nanoparticle surface.

Taking $\mu_{\mathrm{el}} = 20D$ (estimated from the radiative lifetime) [27], $\mu_{\mathrm{vib}} = 10^{-3}D$ and $\gamma = 300\ \mathrm{cm}^{-1}$ [26], $R = 3$ nm (equals the size of the nanoparticle with the passivation layer), $k = 8$, $d_0 = 1/2$ nm, and $n = 1.5$, Eq. (1) results in $\Gamma_{\mathrm{EVET}} \approx 1.5 \times 10^6\ \mathrm{s}^{-1}$. This rough estimate of $\tau \approx 600$ ns is in agreement with the experimental nonradiative transfer lifetimes of 500–1500 ns. This qualitative agreement and the observed experimental resonant behavior provide strong support for the plausibility of the long-range EVET mechanism.

This observation of long-range EVET is uniquely possible in QDs owing to the possibility of tuning through the overtone resonance via changing the nanoparticle (core) size. The dipole-dipole long-range interaction, although weak on a single molecule level, has a cumulative effect from the presence of many solvent molecules surrounding the nanoparticle and is also of relevance to these systems since the radiative lifetimes are on the order of a few hundred ns. At the NIR range, where QDs are potential components in optoelectronic devices, this mode of interaction with the solvent should also be taken into account in the device structure. Even in the common thin film polymer devices incorporating nanoparticles, where ''trivial'' matrix absorptivity is negligible, the EVET process will be active.

Support of the Ministry of Science Tashtiot program and the Converging Technologies Program of The Israel Science Foundation (Grant No. 1704/07) is acknowledged.

*Corresponding author.
banin@chem.ch.huji.ac.il

[1] M. Bixon and J. Jortner, J. Chem. Phys. **48**, 715 (1968); R. Englman, *Non-Radiative Decay of Ions and Molecules in Solids* (North-Holland, Amsterdam, 1979); in *Radiationless Processes in Molecules and Condensed Phases*, edited by F. K. Fong (Springer, Berlin, 1976); J. Jortner and M. Bixon, in *Femtochemistry and Femtobiology*, edited by V. Sundstrum, Nobel Symposium Vol. 101 (Imperial College Press, London, 1997), p. 349; A. Nitzan, *Chemical Dynamics in Condensed Phase* (Oxford University Press, Oxford, 2006).
[2] R. Kubo and Y. Toyozawa, Prog. Theor. Phys. **13**, 160 (1955).
[3] R. A. Marcus, J. Chem. Phys. **24**, 966 (1956).
[4] M. Bixon and J. Jortner, Adv. Chem. Phys. **106**, 35 (1999).
[5] C. Silva, P. K. Walhout, K. Yokoyama, and P. F. Barbara, Phys. Rev. Lett. **80**, 1086 (1998).
[6] Th. Förster, Discuss. Faraday Soc. **27**, 7 (1959).
[7] G. D. Scoles, Annu. Rev. Phys. Chem. **54**, 57 (2003).
[8] N. Tessler, V. Medvedev, M. Kazes, S. Kan, and U. Banin, Science **295**, 1506 (2002).
[9] O. Solomeshch *et al.*, J. Appl. Phys. **98**, 074310 (2005).
[10] J. S. Steckel, S. Coe-Sullivan, V. Bulovic, and M. G. Bawendi, Adv. Mater. **15**, 1862 (2003).
[11] S. A. McDonald *et al.*, Nat. Mater. **4**, 138 (2005).
[12] See E. Rabani *et al.*, J. Chem. Phys. **110**, 5355 (1999) for a description of the effects of the environment on the optical properties of QDs.
[13] A. Aharoni, T. Mokari, I. Popov, and U. Banin, J. Am. Chem. Soc. **128**, 257 (2006).
[14] D. W. Smith *et al.*, Adv. Mater. **14**, 1585 (2002).
[15] Y. K. Olsson *et al.*, Appl. Phys. Lett. **85**, 4469 (2004).
[16] C. K. N. Patel, A. C. Tam, and R. J. Kerl, J. Chem. Phys. **71**, 1470 (1979).
[17] I. Hanazaki, M. Baba, and U. Nagashima, J. Phys. Chem. **89**, 5637 (1985).
[18] A. F. van Driel *et al.*, Phys. Rev. Lett. **95**, 236804 (2005).
[19] D. Schooss, A. Mews, A. Eychmuller, and H. Weller, Phys. Rev. B **49**, 17072 (1994).
[20] U. Banin *et al.*, J. Chem. Phys. **109**, 2306 (1998).
[21] A. J. Williamson and A. Zunger, Phys. Rev. B **61**, 1978 (2000).
[22] D. Krapf, S. H. Kan, U. Banin, O. Millo, and A. Sa'ar, Phys. Rev. B **69** 073301 (2004).
[23] S. A. Egorov, E. Rabani, and B. J. Berne, J. Chem. Phys. **110**, 5238 (1999); S. A. Egorov, E. Rabani, and B. J. Berne, J. Phys. Chem. B **103**, 10 978 (1999).
[24] F. K. Fong, S. L. Naberhuis, and M. M. Miller, J. Chem. Phys. **56**, 4020 (1972).
[25] Y. Weissman, A. Nitzan, and J. Jortner, Chem. Phys. **26**, 413 (1977).
[26] M. S. Burberry, J. A. Morrell, A. C. Albrecht, and R. I. Swoffort, J. Chem. Phys. **70**, 5522 (1979).
[27] P. Yu *et al.*, J. Phys. Chem. B **109**, 7084 (2005).